NeuroImage: Clinical 35 (2022) 103075

Contents lists available at ScienceDirect

NeuroImage: Clinical

journal homepage: www.elsevier.com/locate/ynicl

Neural substrates of psychosis revealed by altered dependencies between brain activity and white-matter architecture in individuals with 22q11 deletion syndrome

Karin Bortolin [a,b,1], Farnaz Delavari [a,b,1,*], Maria Giulia Preti [b,c,d], Corrado Sandini [a], Valentina Mancini [a], Emeline Mullier [e], Dimitri Van De Ville [b,c,d], Stephan Eliez [a,f]

[a] Developmental Imaging and Psychopathology Laboratory, University of Geneva School of Medicine, Geneva, Switzerland
[b] Medical Image Processing Laboratory, Institute of Bioengineering, École Polytechnique Fédérale de Lausanne, Lausanne, Switzerland
[c] Department of Radiology and Medical Informatics, University of Geneva, Geneva, Switzerland
[d] CIBM Center for Biomedical Imaging, Lausanne, Switzerland
[e] Autism Brain and Behavior Laboratory, Department of Psychiatry, University of Geneva, Geneva, Switzerland
[f] Department of Genetic Medicine and Development, University of Geneva School of Medicine, Geneva, Switzerland

ARTICLE INFO

Keywords:
Psychosis
22q11 Deletion syndrome
fMRI
dMRI
Graph signal processing
Function-structure dependency

ABSTRACT

Background: Dysconnectivity has been consistently proposed as a major key mechanism in psychosis. Indeed, disruptions in large-scale structural and functional brain networks have been associated with psychotic symptoms. However, brain activity is largely constrained by underlying white matter pathways and the study of function-structure dependency, compared to conventional unimodal analysis, allows a biologically relevant assessment of neural mechanisms. The 22q11.2 deletion syndrome (22q11DS) constitutes a remarkable opportunity to study the pathophysiological processes of psychosis.

Methods: 58 healthy controls and 57 deletion carriers, aged from 16 to 32 years old, underwent resting-state functional and diffusion-weighted magnetic resonance imaging. Deletion carriers were additionally fully assessed for psychotic symptoms. Firstly, we used a graph signal processing method to combine brain activity and structural connectivity measures to obtain regional structural decoupling indexes (SDIs). We use SDI to assess the differences of functional structural dependency (FSD) across the groups. Subsequently we investigated how alterations in FSDs are associated with the severity of positive psychotic symptoms in participants with 22q11DS.

Results: In line with previous findings, participants in both groups showed a spatial gradient of FSD ranging from sensory-motor regions (stronger FSD) to regions involved in higher-order function (weaker FSD). Compared to controls, in participants with 22q11DS, and further in deletion carriers with more severe positive psychotic symptoms, the functional activity was more strongly dependent on the structure in parahippocampal gyrus and subcortical dopaminergic regions, while it was less dependent within the cingulate cortex. This analysis revealed group differences not otherwise detected when assessing the structural and functional nodal measures separately.

Conclusions: Our findings point toward a disrupted modulation of functional activity on the underlying structure, which was further associated to psychopathology for candidate critical regions in 22q11DS. This study provides the first evidence for the clinical relevance of function-structure dependency and its contribution to the emergence of psychosis.

Abbreviations: FSD, Functional structural Dependency; SDI, Sturctural Decoupling Index; ACC, Anterior Cingulate Cortex; PFC, Prefrontal Cortex; EC, Entorhinal Cortex; AC, Auditory Cortex; 22q11DS, 22q11 Deletion Syndrome.

* Corresponding author at: Campus Biotech, 9 chemin des Mines, 1202 Geneva, Switzerland.
E-mail addresses: Farnaz.Delavari@unige.ch (F. Delavari), maria.preti@epfl.ch (M.G. Preti), corrado.sandini@unige.ch (C. Sandini), valentina.mancini@unige.ch (V. Mancini), dimitri.vandeville@epfl.ch (D. Van De Ville), stephan.eliez@unige.ch (S. Eliez).

[1] These authors contributed equally to this work.

https://doi.org/10.1016/j.nicl.2022.103075
Received 7 February 2022; Received in revised form 10 May 2022; Accepted 1 June 2022
Available online 8 June 2022
2213-1582/© 2022 The Author(s). Published by Elsevier Inc. This is an open access article under the CC BY-NC-ND license (http://creativecommons.org/licenses/by-nc-nd/4.0/).

1. Introduction

Psychosis is a severe mental illness characterized by hallucinations, delusions and disorganized thoughts. This disorder has a significant impact on the quality of life of patients and their families worldwide (McClellan, 2018; Gore et al., 2011). Extensive research over the years pointed to both genetic and environmental factors contributing to the development of psychosis, but the causes and the underlying neural mechanisms are still largely unknown (Kendler, 2013). The 22q11 deletion syndrome (22q11DS) is a neurogenetic disorder that is among the strongest genetic risk factors for developing psychosis (Biswas and Furniss, 2016). Specifically, approximately 30% to 40% of deletion carriers are diagnosed with schizophrenia by adulthood (Murphy et al., 1999; Lewandowski et al., 2007; Schneider et al., 2014; Schneider et al., 2014). Because 22q11DS is usually diagnosed at a young age due to frequently associated heart or cleft palate malformations (McDonald-McGinn et al., 2015), studies on this population constitute a unique opportunity to map the early stages and the progression of psychosis (Insel, 2010; Lewis and Levitt, 2002). In particular, research on 22q11DS allows to investigate alterations in the neural circuitry that eventually affect sensory and cognitive functions. Indeed, to identify early biomarkers as well as to develop new effective therapies, it is crucial to understand the underlying neurobiological changes associated to the psychopathology.

The brain is constituted of functionally specialized areas that interact together to give rise to perception, cognition and action (Johnson, 2001). Dysconnection of these integrative neural circuits has been consistently proposed as a key mechanism in psychosis (Fornito et al., 2012; Pettersson-Yeo et al., 2011). Accordingly, psychosis is better explained by abnormal interactions between distinct brain areas rather than region specific abnormalities (Stephan et al., 2009). These altered connections have been found at both structural and functional level (McGuire and Frith, 1996; Lawrie et al., 2002; Karbasforoushan and Woodward, 2013; Narr and Leaver, 2015), using diffusion-weighted and functional magnetic resonance imaging (DWI and fMRI), which investigate white-matter pathways and neural activation patterns, respectively. However, by considering the impact of structural and functional connectivity separately, only partial information is yielded which prohibits revealing the complex dynamics of their interaction. Indeed, brain activity is likely to be strongly expressed and constrained by structural white matter pathways (Stiso and Bassett, 2018; Hermundstad et al., 2013; Deco et al., 2013). Therefore, the study of function-structure dependency allows a biologically relevant assessment of behavioral neural mechanisms and has the potential to reveal the neurobiological changes underlying the emergence of psychosis.

The first attempts to characterize the function-structure relationship in healthy subjects involved simple measures of correlation. Specifically, activation time courses from areas with direct structural connections are expected to be statistically more dependent. Indeed, structural connectivity measures have been shown to correlate with brain function (Honey et al., 2010; Honey et al., 2009), and areas that are important hubs of functional connectivity are also found to be key in the structural networks (Sporns et al., 2005). Still, brain structural and function connectomes do not follow a perfect correspondence. This has been partly explained by indirect structural connections formed on a polysynaptic structural network, as well as the dynamic nature of functional connections that is not reflected in static functional connectivity analysis. (Honey et al., 2009; Suárez et al., 2020). In individuals with psychosis, the function-structure relationship is likely to be particularly complex. In patients with schizophrenia, findings on function-structure correspondence reported both higher and lower correspondence compared to healthy subjects (van den Heuvel et al., 2013; Skudlarski et al., 2010; Cocchi et al., 2014). Moreover, a considerable number of large-scale abnormalities of functional networks were only in some cases traceable to underlying anatomical changes (Sporns et al., 2005; Cocchi et al., 2014; Crossley et al., 2016). Such inconsistent findings may be partially due to the inability of linear methods, such as correlation, to model the complexity of function-structure relationship. Recent advances in network science (Atasoy et al., 2018) and graph signal processing (Huang et al., 2018) have led to new measures that link regional brain activity and underlying white matter topology, and that were related to different behavioral domains in healthy individuals (Preti and Van De Ville, 2019; Medaglia et al., 2018). Therefore, these measures have a promising potential to provide insights into brain dysfunction and a better understanding of brain communication mechanisms underlying different behavioral domains.

In this study, we applied a methodology that combines the brain function and structure measures (Preti and Van De Ville, 2019) and investigates how much the brain activity in individual regions is exploiting the underlying available white matter structure. In this way, we quantify the regional function-structure dependency (FSD) in patients with 22q11DS and healthy controls using resting-state functional and diffusion MR images. By employing this approach, we detect regions in patients with 22q11DS, for which the changes of functional activity patterns are not supported by accompanying alterations in underlying structural wiring. Consequently, these regions fail to maintain the level of dependency we would observe in healthy controls. Moreover, we further explored how deviation from the expected normal regional FSD could contribute to explain the severity of positive psychotic symptoms. We hypothesized to observe diffuse whole-brain alterations regarding both higher and lower exploitation of underlying structure by the brain activity. Given that previous studies in psychosis and 22q11DS highlighted dysconnectivity in the prefrontal and temporal cortices (Mattiaccio et al., 2018; Ottet et al., ; Scariati et al., 2014), we expected to find individual differences of FSD associated with positive psychotic symptoms mainly in frontal and temporal lobes.

2. Methods and materials

2.1. Participants

Participants were acquired within the on-going cohort of 22q11DS in Geneva which is extensively described in previously published studies (Delavari et al., 2021; Mancini et al., 2020). In this study, we included a total of N = 57 participants with genetically confirmed diagnosis a of 22q11DS (31 females, age-span: 16–32) and N_c = 58 healthy control subjects (31 females, age-span: 16–29). Diagnosis of 22q11.2 deletion was confirmed following a quantitative fluorescent polymerase chain reaction performed in the Department of Medical Genetics in Geneva. Subjects in the two groups were carefully matched for age and gender. 22qdel carriers were recruited as part of a 22q11DS longitudinal study, while healthy controls amongst siblings of the patients or through the Geneva state school system. To assess the presence of psychotic symptoms, the Structured Interview for Prodromal Syndrome (SIPS) has been administered to the patients with 22q11DS by trained clinicians. For this study, we looked at the five positive symptoms subscales (delusional ideas, suspiciousness, grandiose ideas, perceptual abnormalities/hallucinations and disorganized communication). The severity of each symptom was evaluated assigning one score that ranges from 0 (absent) to 6 (severe). For two subjects this information was not available, therefore they were excluded from the severity of psychosis. Participant's clinical characteristics are further listed in Table 1. Written informed consent was obtained from participants or their parents. The study was approved by the cantonal ethics committee and conducted according to the Declaration of Helsinki.

2.2. MRI acquisition

MRI scans were acquired using a Siemens Trio (n = 108) and a Siemens Prisma-fit (MAGNETOM Trio Upgrade) (n = 7) 3 Tesla scanner. Resting-state fMRI scans were recorded during an 8 min session in which the participants were asked to fixate on a white cross on the screen and

Table 1
Demographic information, presence of psychiatric disorders and drug usage at the moment of the visit in healthy controls and participants with 22q11DS. For the IQ measurements we used Wechsler Intelligence Scale for Children–III (Watkins, 2006) for participants younger than 18 and the Wechsler Adult Intelligence Scale–III (Wechsler, 1955) for the others. To assess the presence of psychiatric disorders we used Clinical interview with the patients using the Diagnostic Interview for Children and Adolescents Revised (Reich, 2000), the psychosis supplement from the Kiddie-Schedule for Affective Disorders and Schizophrenia Present and Lifetime version (Kaufman et al., 1997) and the Structured Clinical Interview for DSM-IV Axis I Disorder (First et al., 1997). SD, standard deviation; NA, not available.

Demographic variables	22q11DS	Healthy controls	p-value
Number of subjects (F/M)	57 (31/26)	58 (31/27)	0.93
Scanner type: Prisma-fit/Trio	3/54	4/54	0.71
Average age (SD)	21.38 (3.7)	20.93 (4.2)	0.54
Average IQ (SD)	72.86 (12.93)	112.16 (12.81)	<0.001
Average frame-wise displacement after scrubbing (SD)	0.17 (0.06)	0.12 (0.04)	<0.001
Anxiety disorder (%)	31 (54.4%)	0	NA
Attention deficit hyperactivity disorder (%)	8 (14%)	0	NA
Mood disorder (%)	10 (17.5%)	0	NA
Schizophrenia spectrum disorders (%)	5 (8.8%)	0	NA
More than one psychiatric comorbidity (%)	13 (22.8)	0	NA
Anticonvulsants (%)	1 (1.7%)	0	NA
Antidepressants (%)	2 (3.5%)	0	NA
Neuroleptic (%)	8 (14%)	0	NA
Psychostimulant (%)	19 (33.33%)	0	NA
Anxiolytic (%)	3 (5.2%)	0	NA

not to fall asleep. fMRI images were acquired using a T2-weighted sequence (200 frames) and the following parameters: acquisition matrix = 94 × 128, field of view = 96x128, voxel size = 1.84 × 1.84 × 3.2 mm^3, 38 axial slices, slice thickness = 3.2 mm, TR = 2400 ms, TE = 30 ms, flip angle = 85°, phase encoding A ≫ P, descending sequential ordering, GRAPPA acceleration mode with factor PE = 2. Diffusion MRI (dMRI) images were acquired along 30 directions using the following sequence parameters: b = 1000 s/mm^2, volumetric resolution = 2x2x2 mm^3, TR = 8300 ms to 8800 ms, TE = 84 ms, flip angle = 90° to 180°, acquisition matrix = 128 × 128, field of view = 25.6 cm, 64 axial slices, slice thickness = 2 mm. A T1-weighted sequence with 192 slices provided anatomical images necessary for the processing of functional and dMRI images (sequence parameters: volumetric resolution = 0.86 × 0.86 × 1.1 mm^3, TR = 2500 ms, TE = 3 ms, flip angle = 8°, acquisition matrix = 256 × 256, slice thickness = 1.1 mm).

2.3. fMRI processing

Statistical Parametric Mapping (SPM12, Wellcome Trust Centre for Neuroimaging, London, UK: http://www.fil.ion.ucl.ac.uk/spm/), and functions of the Data Processing Assistant for Resting-State fMRI (DPARSF) were used in order to perform the fMRI preprocessing steps. For each participant, functional images were first realigned over time and spatially smoothed with an isotropic Gaussian kernel of 5 mm full width half maximum (FWHM). Subsequently, anatomical images were coregistered to the functional space and segmented with the SPM12 Segmentation algorithm (Ashburner and Friston, 2005). Brainnetome's parcellation (https://atlas.brainnetome.org) was resliced to fMRI resolution in order to parcellate the functional images into $N_R = 246$ regions of interest (ROI) including cortical and subcortical areas. Nuisance variables were regressed out (6 head motion parameters + other 6, average cerebrospinal fluid, and white matter signal). The first five functional images were excluded and the voxel fMRI time courses were filtered with a bandwidth of 0.01 Hz to 0.1 Hz. In order to obtain regional fMRI time courses, BOLD signals were averaged across all the voxels included in each Brainnetome region. Motion scrubbing (Power et al., 2012) was finally applied for the correction of motion artifacts based on the framewise displacement (FD), which is defined as the sum of the absolute values of the six realignment parameters. When FD was>0.5 mm, the time point itself, the previous and two consecutive time points were excluded from the analysis. Finally, regional preprocessed time-courses were z-scored. One very small subnucleus of the left thalamus was removed from the current analysis due to its reduced size resulting in no overlap with individual cortices after registration to the individual space and masking (hence, $N_R = 245$ for the following). Finally, for each participant we obtained a functional connectome constituted out of pairwise Pearson's correlation between regional time courses. Functional node strength for each region was computed as the sum of absolute correlation values.

2.4. dMRI processing

After visual inspection for motion artefacts, dMRI images were preprocessed and registered to T1 images using Connectome Mapper 3 (https://connectome-mapper-3.readthedocs.io/en/latest/index.html) which is a open-source image processing pipeline software using a combination of libraries such as MRtrix3 (https://www.mrtrix.org/) and FSL (Jenkinson et al., 2012). Subsequently, the following steps of the processing including the warping of the Brainnetome atlas and the generation of the connectome were performed using in-house pipeline. In this section, we report the details of this pipeline.

Firstly, dMRI images were denoised using the MP-PCA algorithm in MRtrix (Veraart et al., 2016; Veraart et al., 2016; Cordero-Grande et al., 2019). Images were corrected for eddy currents and motion using eddy algorithm in FSL (Andersson and Sotiropoulos, 2016). Then, the T1 anatomical images were registered to diffusion space using a non-linear registration method (ANTs) with the algorithm SyN (Avants et al., 2008) and were segmented into cortical gray matter, subcortical gray matter, white matter and CSF using Freesurfer. The Brainnetome atlas was warped from MNI to anatomical subject-space and down-sampled to dMRI resolution using FSL-FNIRT (Andersson et al., 2007). Fiber orientation distribution was estimated using a constrained spherical deconvolution with single-shell single-tissue response function using the csd algorithm in MRtrix (Tournier et al., 2007). Probabilistic fiber tracking was applied to reconstruct 10^6 streamlines using the tckgen function in MRtrix with the following parameters: step size of 0.5, angle of 45, maximum length of 250 mm, a cutoff of 0.06. Anatomically-Constrained Tractography framework during tracking was also used (Smith et al., 2012). Subsequently, the tractogram was filtered using spherical-deconvolution informed filtering of tractograms 2 (SIFT2) (Smith et al., 2015) for each subject. The structural connectomes were obtained by calculating the number of streamlines linking every pair of the $N_R = 245$ regions defined for the functional analysis, divided by the total number of streamlines. Finally, in order to quantify the structural node strengths, for each participant we computed the sum of each row of the structural connectome.

2.5. Function-structure dependency

For each participant, we calculated the structural decoupling index (SDI) for every region, using the graph-signal-processing methodological pipeline detailed in (Preti and Van De Ville, 2019). In brief, structural harmonics; (i.e., brain patterns that most naturally encode the wiring architecture), were obtained by the eigendecompostion of the normalized Laplacian of an individual's structural connectome. This yielded N_R Laplacian eigenvectors, so called harmonic components, each of which is associated to an eigenvalue that can be interpreted as a graph frequency value. Harmonic components with low graph frequencies are, by construction, 'easier' to express on the structural connectome; i.e., they represent global brain patterns along the main

geometrical axes such as anterior-posterior or left–right. While the components associated with higher graph frequencies are capturing more complex and localized patterns. We subsequently projected the individual functional data, for each time point, onto the individual structural harmonics and applied a graph signal filtering that decomposes the activity signal into two parts: one expressed on low-frequency structural harmonics (and therefore more aligned with structure), and the other one on the complementary high-frequency ones (hence, more detached from structure). The cut-off frequency of the ideal low-/high-pass filter is defined by an equal-energy split of the energy spectral density of each subject. The norm across time of aligned and detached signal portions was computed and their ratio yielded the SDI. It is noteworthy the term structural decoupling index is not to be confused with use of the term "coupling" in the field of neuromodulation. SDI quantifies the absence of function-structure dependency in each region. Therefore, brain areas with an SDI > 1 are regions whose activity signals are relatively more divergent from underlying structural pathways and thus have lower FSD, and the opposite occurs for regions with SDI < 1.

2.6. Statistical analysis

In order to identify for which brain regions of the brain nodal functional connectivity strength, nodal structural connectivity strength, or the SDI significantly differ in participants with 22q11DS and healthy controls, we used a two-sample unpaired *t*-test for normal distributions, or the non-parametric test named Wilcoxon rank sum test in case of non-normal distributions. (More information regarding the test for normality is presented in supplementary materials. Table S3) We corrected the results for multiple comparisons using False Discovery Rate (FDR) correction (Benjamini and Hochberg, 1995). Age and motion (average FD after scrubbing) were included as nuisance regressor in group comparisons. Further, to investigate the implication of individual differences of SDI in the severity of positive psychotic symptoms, we applied a behavioral Partial Least Squares Correlation (PLS-C) analysis (McIntosh and Lobaugh, 2004; Krishnan et al., 2011) using myPLS toolbox (https://github.com/danizoeller/myPLS). PLS-C is a multivariate approach that aims at finding linear combinations of the original data (i.e., latent components) maximizing the covariance between brain and behavioral data, represented in our case by the SDI in patients with 22q11DS and seven behavioral variables corresponding to five positive psychotic symptoms subscales scores, sex, and age. Before entering the SDI and the behavioral measures into PLS-C, motion (average FD after scrubbing) was regressed out for each variable separately. As a result, we obtained brain and behavioral saliences, indicating the importance of each brain region or each behavioral score, respectively, in characterizing the correlation between SDI and the presence of positive psychotic symptoms. The significance of latent components was determined by 1000 permutations. Moreover, we evaluated the stability of the brain and behavioral saliences implementing a bootstrap procedure consisting of 500 random samples with replacement. The brain pattern is visualized choosing bootstrap ratio scores (BRS) that are in absolute value >2.3, corresponding to a confidence level of approximately 95%. Instead, the behavioral saliences are presented as bar plots with the related 95% confidence interval bars according to each bootstrap distribution. In order to assess the effectiveness of SDI, a PLS-C has also been performed for both the functional and structural connectivity node strength measures separately.

3. Results

3.1. Function-structure dependency

The multimodal analysis in healthy controls (HCs) and patients

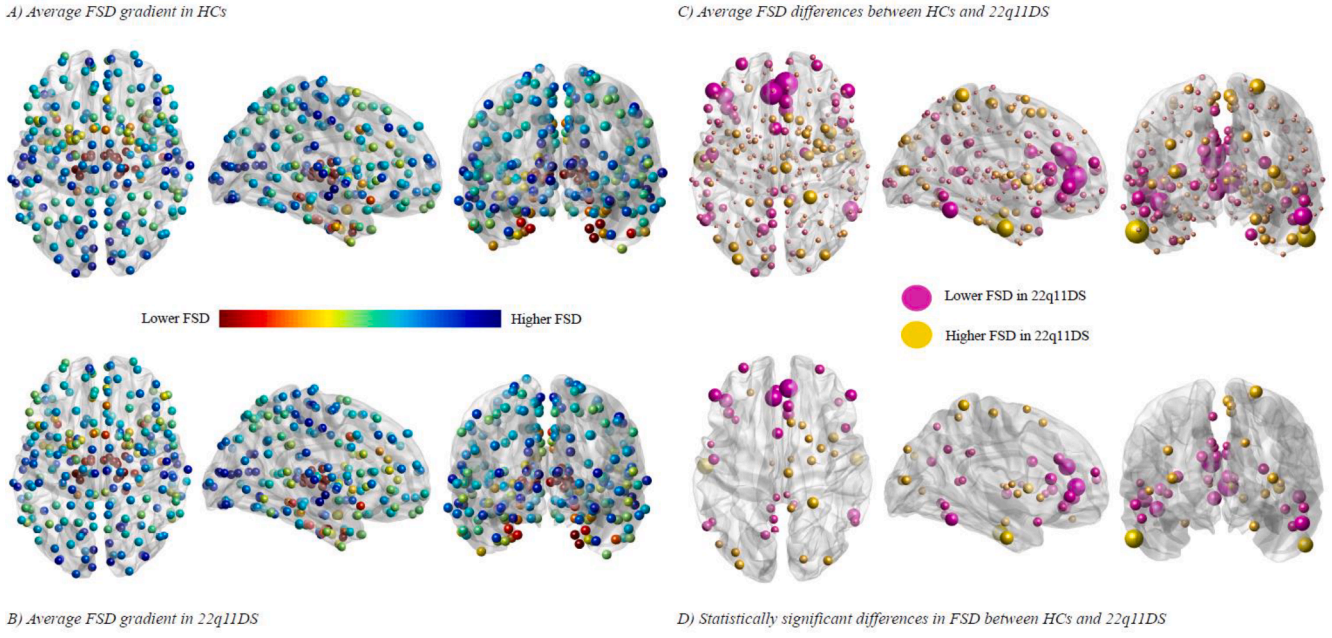

Fig. 1. Comparison between the brain SDI gradient of healthy controls and participants with 22q11DS. **(A)** The binary logarithm of the average SDI calculated for the healthy controls. **(B)** The binary logarithm of the average SDI calculated for the participants with 22q11DS. In A) and B) primary sensory cortices present the strongest FSD (low values of SDI - dark blue points), frontal cortex exhibits moderate FSD (green and light blue points), while inferior temporal cortex and subcortical regions present the weakest FSD (high values of SDI - red points). Thus, the gradient of FSD as in sensory cortices > frontal cortices > subcortical cortices, is consistently present in both groups. **(C)** Brain map of the differences between the binary logarithm of average SDI of healthy controls and the binary logarithm of the average SDI of participants with 22q11DS. Compared to healthy controls, participants with 22q11DS present stronger FSD in occipital, inferior temporal, superior frontal lobes and subcortical areas (yellow regions). Concurrently, FSD is weaker mainly in prefrontal and superior temporal cortices (pink regions). **(D)** Statistically significant SDI group differences after correction for multiple comparisons. In C) and D), the dimension of the points depicts the magnitude of the regional SDI difference in binary logarithm form, which could be viewed as the relative difference across the two groups (detailed in supplementary material Table S.3). (For interpretation of the references to colour in this figure legend, the reader is referred to the web version of this article.)

generated a macroscale gradient of SDI over the whole brain (Fig. 1A and 1B). The cortical gradient revealed regions in visual, sensory, motor and auditory cortices had the lowest SDI values (dark blue nodes) indicating a strong alignment between function and structure (high FSD). On the contrary, cortices dedicated to higher-level cognitive function mainly located in the frontal and temporal lobes (light blue, yellow and light red nodes) presented relatively higher SDI values, indicating relatively lower FSD. These results were in line with findings in previous work (Preti and Van De Ville, 2019), except that the inclusion of subcortical brain regions showed that the FSD further decreases for regions such as amygdala, hippocampus, thalamus and basal ganglia (highest SDI values - dark red nodes), for which the functional activity is the least constrained by the underlying anatomical backbone.

Table 2

Brainnetome atlas regions for which the average SDI is significantly different between healthy subjects and participants with 22q11DS. The first column indicates the region's location in the brain, while the second column indicates the brain region's name (BA = Brodmann Area) with the correspondent region's IDs of the Brainnetome atlas (third column). The average SDI value for healthy controls (*SDI_HC*), the average SDI value for participants with 22q11DS (*SDI_22q11DS*), the adjusted p-values (q-value) after correction for multiple comparisons are also list in the following columns. Finally, we report in the last columns the average structural nodal strength which consists of sum of all connections for a certain region. Structural nodal strength was reported for healthy controls (*SC_HC*) and for 22q11DS (*SC_22q11DS*) with the respective adjusted p-value (q-value) after multiple comparisons. For region withs significantly different SDI values, the average correlation coefficient between SDI and motion (in terms of mean frame-wise displacement after scrubbing) is reported.

Higher average FSD in 22q11DS *(SDI_22q11DS < SDI_HC)*								
Region's location	**Region's name (hemisphere)**	**Region's ID**	SDI_HC	SDI_22q11DS	**q-value (FDR)**	SC_HC	SC_22q11DS	**q-value (FDR)**
Superior Frontal Gyrus	*medial BA 8 (L)*	2	0.92	0.80	0.0153	0.0048	0.0052	>0.05
	dorsolateral BA 6 (R)	8	1.10	0.97	0.0325	0.0045	0.0049	0.0428
Orbital Gyrus	*lateral BA 11 (L)*	45	0.92	0.82	0.0325	0.0062	0.0072	0.0004
Paracentral Lobule	*BA 4 (R)*	68	0.67	0.58	0.0195	0.0042	0.0043	>0.05
Inferior Temporal Gyrus	*intermediate lateral BA 20 (L)*	95	1.43	1.14	0.0133	0.0015	0.0021	0.0000
	intermediate lateral BA 20 (R)	96	1.28	1.05	0.0139	0.0017	0.0021	0.0284
Superior Parietal Lobule	*postcentral BA 7 (R)*	132	0.93	0.78	0.0071	0.0038	0.0041	>0.05
Inferior Parietal Lobule	*caudal BA 39 (L)*	135	0.83	0.73	0.0150	0.0053	0.0057	>0.05
Precuneus	*medial BA 5 (L)*	150	0.82	0.72	0.0325	0.0040	0.0037	>0.05
Insular Gyrus	*dorsal granular insula (R)*	172	0.84	0.75	0.0324	0.0024	0.0027	0.0063
	dorsal dysgranular insula (R)	174	0.78	0.66	0.0409	0.0024	0.0030	0.0000
Lateral Occipital Cortex	*middle occipital gyrus (L)*	199	0.69	0.59	0.0116	0.0056	0.0053	>0.05
	middle occipital gyrus (R)	200	0.68	0.58	0.0195	0.0049	0.0048	>0.05
	BA V5/MT+ (L)	201	0.97	0.87	0.0409	0.0050	0.0048	>0.05
	medial superior occipital gyrus (R)	208	0.80	0.70	0.0139	0.0052	0.0048	0.0373
Hippocampus	*rostral hippocampus (R)*	216	0.78	0.68	0.0228	0.0052	0.0051	>0.05
Basal Ganglia	*ventral caudate (R)*	220	0.95	0.83	0.0116	0.0052	0.0060	0.0000
	dorsolateral putamen (R)	230	0.85	0.75	0.0071	0.0079	0.0087	0.0000
Thalamus	*medial pre-frontal thalamus (R)*	232	2.62	2.36	0.0149	0.0013	0.0015	0.0006
	rostral temporal thalamus (R)	238	2.06	1.87	0.0409	0.0025	0.0024	>0.05
Lower average FSD in 22q11DS *(SDI_22q11DS > SDI_HC)*								
Region's location	**Region's name (hemisphere)**	**Region's ID**	SDI_HC	SDI_22q11DS	**q-value (FDR)**	SC_HC	SC_22q11DS	**q-value (FDR)**
Middle Frontal Gyrus	*BA 46 (L)*	19	0.78	0.92	0.0089	0.0046	0.0047	>0.05
	BA 46 (R)	20	0.71	0.82	0.0090	0.0044	0.0047	>0.05
Inferior Frontal Gyrus	*rostral BA 45 (L)*	35	0.84	1.03	0.0022	0.0025	0.0026	>0.05
	rostral BA 45 (R)	36	0.85	1.02	0.0071	0.0025	0.0025	>0.05
	opercular BA 44 (L)	37	0.72	0.85	0.0071	0.0035	0.0035	>0.05
Orbital Gyrus	*lateral BA 12/47 (L)*	51	0.57	0.71	0.0003	0.0048	0.0054	0.0000
	lateral BA 12/47 (R)	52	0.68	0.78	0.0332	0.0037	0.0042	0.0001
Precentral Gyrus	*BA 4*							
(tongue and larynx region) (L)	61	0.71	0.79	0.0325	0.0035	0.0037	>0.05	
Auditory Cortex	*TE1.0 and TE1.2 (L)*	73	0.56	0.66	0.0078	0.0039	0.0039	>0.05
Superior Temporal Gyrus	*lateral BA 38 (R)*	78	0.89	1.03	0.0230	0.0027	0.0028	>0.05
Inferior Temporal Gyrus	*extreme lateroventral BA37 (L)*	91	0.75	0.86	0.0484	0.0030	0.0030	>0.05
	extreme lateroventral BA37 (R)	92	0.84	1.03	0.0253	0.0017	0.0015	>0.05
	ventrolateral BA 37 (L)	97	0.91	1.06	0.0205	0.0033	0.0031	>0.05
	ventrolateral BA 37 (R)	98	0.95	1.10	0.0228	0.0027	0.0024	0.0297
Precuneus	*medial BA 7 (L)*	147	0.77	0.87	0.0149	0.0034	0.0031	>0.05
	medial BA 5 (L)	151	0.46	0.54	0.0025	0.0069	0.0059	0.0000
	BA 31 (L)	153	0.66	0.75	0.0149	0.0054	0.0051	>0.05
Insular Gyrus	*dorsal agranular insula (L)*	167	1.14	1.29	0.0196	0.0019	0.0019	>0.05
	dorsal BA 23 (L)	175	0.90	1.01	0.0186	0.0034	0.0032	>0.05
	dorsal BA 23 (R)	176	0.97	1.08	0.0189	0.0030	0.0027	0.0041
Cingulate Cortex	*rostroventral BA 24 (L)*	177	0.89	1.06	0.0071	0.0047	0.0048	>0.05
	rostroventral BA 24 (R)	178	0.69	0.83	0.0027	0.0066	0.0065	>0.05
	pregenual BA 32 (L)	179	0.96	1.22	0.0000	0.0027	0.0023	0.0000
	pregenual BA 32 (R)	180	1.17	1.40	0.0055	0.0021	0.0017	0.0000
	ventral BA 23 (L)	181	0.75	0.86	0.0183	0.0045	0.0044	>0.05
	ventral BA 23 (R)	182	0.79	0.89	0.0440	0.0039	0.0038	>0.05
	subgenual BA 32 (L)	187	0.75	0.91	0.0022	0.0043	0.0039	0.0284
	subgenual BA 32 (R)	188	0.88	1.13	0.0000	0.0025	0.0021	0.0011

Framewise displacement correlation with SDI			
Correlation coefficient (r-value), Average (standard deviation)			**P- value**
Areas with significantly different SDI in the groups	**HC**	**22q11DS**	
	2.46e-17 (1.02e-16)	4.32e-18 (7.63e-17)	0.3502

3.2. Comparing participants with 22q11DS against healthy controls

The map of whole brain average SDI differences (defined as SDI_HC–SDI_22q11DS) is presented in Fig. 1C. Comparing the average regional SDI between patients with 22q11DS and HCs, 48 out of 245 brain regions remained significantly different across the groups after multiple comparisons correction (Fig. 1D). Regions with significantly higher FSD in patients with 22q11DS (yellow nodes) were mainly clustered in inferior temporal, superior parietal, lateral occipital cortex and subcortical areas. Conversely, prefrontal regions along with cingulate cortex presented a weaker FSD (pink nodes) in participants affected by the deletion when compared with HCs. Table 2, presents the average SDI values in both groups and the respective p-values after multiple comparison. Additionally, for the depicted regions, correlation of motion variable (frame-wise displacement after scrubbing) and SDI within each region in both groups of 22q11DS and healthy controls was calculated. Average correlation coefficient did not differ between patients and healthy controls (Wilcoxon rank sum test, p-value = 0.3502). A more detailed investigation of contribution of motion to SDI is provided in supplementary materials.

3.3. Association with positive psychotic symptoms

PLS-C behavioral analysis resulted in one significant latent component (LC1, p = 0.017), which captured a strong positive effect of all the five positive psychotic symptoms, a small negative effect of gender and no effect of age (Fig. 2B). Thus, the corresponding brain saliences (Fig. 2A) mainly display a pattern in which SDI is broadly associated with the severity of psychosis. The brain activity of patients experiencing higher scores of psychotic symptoms is less dependent on the white matter structure in the anterior cingulate cortex (ACC), thalamus and parietal lobule (red regions in Fig. 2A). On the contrary, brain activity is more aligned with structure in inferior and superior temporal gyrus, parahippocampal gyrus, and putamen (blue regions in Fig. 2A).

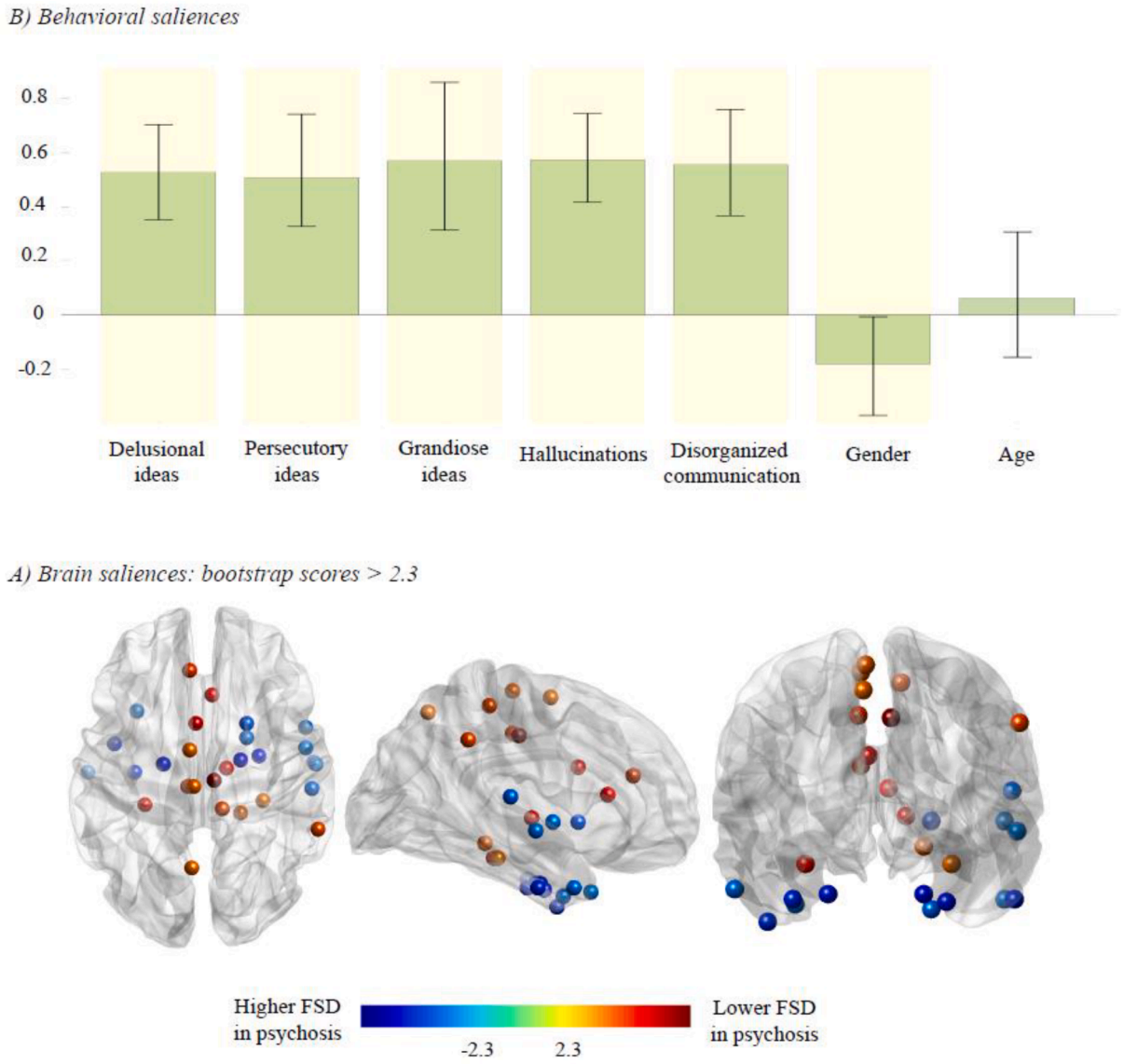

Fig. 2. Individual differences in SDI are significantly associated with the severity of positive psychotic symptoms in participants with 22q11DS. Brain and behavioral saliences relative to the significant LC resulted from the PLS-C analysis are displayed. (A) The pattern of brain saliences shows that compared to deletion carriers experiencing mild or no positive psychotic symptoms, the ones presenting severe symptoms exhibit stronger FSD in the parahippocampal and inferior temporal gyrus (blue regions). Concurrently, FSD is weaker mainly in the cingulate gyrus and in the parietal cortex (red regions). (B) The design saliences reveal a strong positive effect of all the five positive symptoms subscales, a small effect for gender and no effect for age. (For interpretation of the references to colour in this figure legend, the reader is referred to the web version of this article.)

Each specific atlas region with the correspondent salience value is listed in Table 3. Additionally, we conducted a supplementary PLS including a variable for consumption of psychostimulants, which did not produce a robust loading (Fig. 4S).

3.4. Contribution of unimodal measures

In terms of node strengths of the functional connectome, no significant group difference was found. On the contrary, differences among the node strengths of the structural connectome were found across all the brain (75 regions out of 245). In Table 2, the structural nodal values and the respective p-values after multiple comparisons correction are listed for each region in which the SDI values were significantly different. The regions in which we found different structural nodal strengths between the two groups are visible in Fig. 1S of supplementary materials. PLS-C analysis performed for functional and structural node strength measures separately in both cases resulted in no significant components. Of note, to explore an approach already used in previous literature we further examined the connectomes in terms of connectivity measures. Thus, we performed an independent *t*-test analysis for each ROI-to-ROI connection within the functional and structural connectomes. Results for group differences among structural and functional connections, after correcting for multiple comparisons, are reported in Fig. 2S and 3S.

Table 3
Brainnetome atlas regions for which the SDI values were significantly associated with the severity of positive psychotic symptoms in 22q11DS. The first column indicates the region's location in the brain, while the second column indicates the brain region's name (BA = Brodmann Area) with the correspondent region's IDs of the Brainntetome atlas (third column). The brain salience value associated to the correspondent region is also listed (fourth column): positive values indicate that deletion carriers with more severe psychotic symptoms present weaker FSD, while negative values indicate they present stronger FSD.

Higher FSD in deletion carriers experiencing positive psychotic symptoms			
Region's Location	**Region's name (hemisphere)**	**Region's ID**	**Brain salience**
Superior Temporal Gyrus	*medial BA 38 (L)*	69	−2.44
	BA 41/42 (R)	72	−2.48
	TE1.0 and TE1.2 (R)	74	−2.34
	rostral BA 22 (R)	80	−2.36
	rostral BA 21 (R)	84	−2.46
Inferior Temporal Gyrus	*rostral BA 20 (L)*	93	−3.32
	intermediate lateral BA 20 (L)	95	−2.47
	intermediate lateral BA 20 (R)	96	−3.09
	rostroventral BA 20 (L)	103	−3.23
Parahippocampal Gyrus	*rostral BA 35/36 (R)*	110	−3.54
	BA 28/34 (entorhinal cortex) (L)	115	−3.35
	BA 28/34 (entorhinal cortex) (R)	116	−3.45
	temporal agranular insular cortex (R)	118	−2.52
Basal Ganglia	*ventromedial putamen (R)*	226	−2.85
Lower FSD in deletion carriers experiencing positive psychotic symptoms			
Region's Location	**Region's name (hemisphere)**	**Region's ID**	**Brain salience**
Superior Frontal Gyrus	*medial BA 6 (L)*	9	2.53
	medial BA 6 (R)	10	2.32
Paracentral Lobule	*BA1/2/3 (lower limb region) (R)*	66	2.67
	BA 4 (L)	67	2.49
Parahippocampal Gyrus	*posterior parahippocampal gyrus (L)*	113	3.34
	posterior parahippocampal gyrus (R)	114	2.35
	area TH (medial PPHC) (R)	120	2.63
Inferior Parietal Lobule	*caudal BA 40 (R)*	142	2.78
Precuneus	*medial BA 7 (L)*	147	2.50
Cingulate Gyrus	*rostroventral BA 24 (L)*	177	4.04
	rostroventral BA 24 (R)	178	3.38
	pregenual BA 32 (L)	179	3.14
	caudal BA 23 (L)	185	2.89
	caudal BA 23 (R)	186	4.89
Thalamus	*sensory thalamus (R)*	234	3.70

4. Discussion

In line with previous findings in healthy adults reported in Preti et al. (Preti and Van De Ville, 2019); our analysis revealed a major spatial gradient ranging from sensory-motor regions (stronger FSD) to regions involved in higher-order function (weaker FSD); see Fig. 1A and 1B. Similarly, multiple studies have already reported a comparable gradient that spans from strongly aligned 'unimodal' sensory cortices to weakly aligned 'trans-modal' cortices using different measures (Margulies et al., 2016; Vázquez-Rodríguez et al., 2019; Baum et al., 2020; Paquola et al., 2019). This hierarchical organization of the brain has been proposed to support increasing levels of flexible and dynamic processes. Accordingly, polysynaptic indirect connections are more likely to be involved in higher-order integrative processes (Buckner and Krienen, 2013). Brain areas at the apex of the hierarchy may activate more in synchrony, not only as a consequence of direct signaling between them, but also by being driven by common inputs received from the rest of the brain. Consequently, the simultaneous functional activation of regions that are not structurally linked leads to a weak FSD (Bettinardi et al., 2017; Damoiseaux and Greicius, 2009). On the contrary, in sensory regions the functional activity could be more directly supported by the underlying white matter pathways because of the need for fast reactions to internal or external stimuli (Mesulam, 1998). Furthermore, by adding the subcortical regions we observed that functional activity is even less constrained by anatomical backbone compared to frontal and temporal *trans*-modal cortices. These regions are involved in complex and polysynaptic circuits (Utter and Basso, 2008; Berridge and Kringelbach, 2015; Janak and Tye, 2015) and the weakest alignment observed further supports the hypothesis that a decrease in function-structure alignment consents increasing flexible and dynamic processes (Mesulam, 1998).

Current knowledge converges on the idea of a hierarchical organization of functional-structural dependency. However, the divergence from a normal FSD within one region and its pathological implications are not well understood yet (Suárez et al., 2020). In the present study, our analysis revealed a similar FSD gradient throughout the brain for both groups of 22q11DS and HCs, which confirmed that the dominant FSD pattern is reflecting a robust organizational principle of the brain. However, when comparing regional FSD between 22q11DS and HCs by means of structural decoupling index, we found a significant difference in several brain areas. A considerable number of regions with lower FSD in 22q11DS were located in the prefrontal cortex (PFC) and ACC, which are well known to play a crucial role in executive function, attention, memory and emotional regulation (Miller and Cohen, 2001). In fact, better executive function has been associated with higher prefrontal FSD (Medaglia et al., 2018). In this context, pruning occurring during normal development of the PFC, may lead to more efficient white matter mediation to support the complex functionality of PFC (Kolb and Gibb, 2011; Hooper et al., 2004). Therefore, sufficiently high FSD in prefrontal areas could be indicative of a well-matured cortex (Mills et al., 2014; Schlegel et al., 20122012). Consequently, the abnormally low FSD detected in 22q11DS in this study, could point to the structural impairments resulting from an abnormal pruning process and immature PFC that does not form the optimal structural connections to support complex executive functions. Structural impairments in prefrontal cortex and abnormal pruning (Shashi et al., 2012; Schaer et al., 2009) have been already documented in 22q11DS (Radoeva et al., 2012) and have been further associated with behavioral dysfunctions and psychotic symptoms (Schreiner et al., 2014). Additionally, our analysis detected abnormally high FSD in striatal area of patients with 22q11DS, which was associated with the severity of psychotic symptoms. Indeed, it has

been already suggested that the abnormal PFC maturation in 22q11DS is driven by dopaminergic dysfunction (Schaer et al., 2009). Notably, insufficient cortical dopamine combined with sub-cortical hyper-dopaminergic state is one of the most accepted mechanism in psychosis (Lodge and Grace, 2007) and it has been recently indicated in 22q11DS (Delavari et al., 2021). In that regard, abnormally high FSD within the striatal area could be indicative of a maximal subcortical dopaminergic activation that saturates the underlying wiring structures.

In addition, our results pointed towards an association between the presentation of positive psychotic symptoms and the decrease of FSD in ACC within participants with 22q11DS. Indeed, ACC has been consistently associated with the presence and severity of psychotic symptoms in both functional and structural neuroimaging studies conducted in patients with 22q11DS (Rihs et al., 2013; Scariati et al., 2016; Sandini et al., 2018; Tomescu et al., 2014; Padula et al.,), as well as idiopathic schizophrenia (Allen et al., 2008; Menon, 2011). Reductions in white matter tracts observed in the ACC of patients with 22q11DS could lead to functional reorganization that finally results in the development of alternative activation patterns, detached from the underlying structural connections. Given that ACC, as part of the salience network, plays an active role in detecting salient stimuli, the detachment we observed in ACC may point towards irrelevant activations, resulting in misattribution of salience (Kapur, 2003). On the other hand, our results further denoted a higher alignment in the entorhinal cortex (EC) of patients with 22q11DS with more severe psychotic symptoms. Notably, EC is part of the novelty detection circuit (Witter et al., 2000), it is connected to ACC via cingulum (Rolls, 2019) and it mediates the input and output of the hippocampus. EC mainly holds sensory information while the hippocampus compares it with internal representations (Falkai et al., 2000; Prasad et al., 2004). Previous studies in schizophrenia found reductions in volume of EC (Arnold, 1999; Bettinardi et al., 2017) and higher activation in parahippocampal gyrus has been previously linked to psychosis (Delavari et al., 2021; Zöller et al., 2017; Boley et al., 2014; Friston et al., 1992). This finding may suggest an over-engagement in the local circuits of hippocampal complex, leading to a disruption of the novelty detection processes. This, along with misattribution of salience has been proposed as a potential mechanism contributing to distortion of reality that is observed in psychosis (Lisman and Otmakhova, 2001).

The relatively elevated FSD values in sensory regions of patients with 22q11DS, may implicate that brain activity is more restricted to local structural circuits and, therefore, these regions are less integrated with higher order cognitive areas. The resulting segregation of the superior parietal and inferior temporal lobe could explain the wide-ranging impairments in sensory domains and visuospatial abilities observed in 22q11DS (Larsen et al., 2019; Bostelmann et al., 2016; Attout et al., 2017). Our analysis isolated the primary auditory cortex (AC), by detecting a lower FSD in 22q11DS as compared to HCs, which is an exception among other sensory areas. Several studies in 22q11DS have shown robust functional hyperactivity in AC, which strongly correlates with the emergence of auditory hallucinations (Mancini et al., 2020; Ferri et al., 2018; Li et al., 2017). Intriguingly, stronger AC alignment was detected in patients presenting more severe positive psychotic symptoms, thus the lower FSD in AC of patients with 22q11DS, was driven by less symptomatic patients. This could be pointing towards a trait, where compensatory integration of auditory circuits has a protective role against positive psychotic symptoms.

Overall, our findings showed abnormal function-structure dependencies within critical regions in individuals with 22q11DS. Notably, when analyzing separately the nodal measures for structural and functional connectomes, we found no significant results. Therefore, the FSD was unique in providing significant associations with psychosis psychopathology. The present study provides first evidence of the clinical relevance of the FSD, highlighting changes that are not otherwise identifiable with a nodal functional or structural analysis alone. These results suggest that the emergence of psychosis may be more tightly related to a disrupted ability of brain networks to modulate functional activation on the underlying white-matter pathways, rather than to separate alterations of nodal structural or functional connections. It is noteworthy that a post-hoc analysis examining the group differences in the ROI-to-ROI connectivity, resulted in statistically significant differences reported in previous literature that explored functional and structural connectivity in participants with 22q11DS. However, here we showed that nodal measures for structural or functional scans, taken separately, fail to reflect the changes expected in participants with 22q11DS. Nevertheless, by combining functional and structural information into the integrative FSD framework led to meaningful results at a nodal level. Therefore, we suggest that the methods assessing functional structural dependency hold a potential to robustly detect differences when performing a regional level analysis.

4.1. Conclusions and further perspectives

By combining information from functional and diffusion MR imaging in a single unified framework, we showed that brain function is differently constrained by the anatomical structure in 22q11DS. However, the findings of this study present some limitations that are worthy to be considered. Firstly, morphometric alterations in 22q11DS impose a limitation in conducting analysis in a normalized template space. To overcome this, we have calculated the SDI in the native subject space. However, atlas realignment are not ideally formed to address morphological alterations in this population.. Furthermore our data consists of dMRI images acquired along 30 directions using a b-value of 1000 s/mm, which are the minimal technical requirements to obtain an optimal tensor estimation (Calamuneri et al., 2018). Certainly, the latest available DSI or HARDI sequences use more gradient directions and higher b-values which results in better reconstruction of crossing fibers (Tournier et al., 2004). Additionally, anatomically-constrained tractography (ACT) and spherical-deconvolution informed filtering of tractograms (SIFT) algorithms were adopted in the tractographic reconstruction of the SC, as shown to produce more biologically realistic connectomes (Smith et al., 2012) and reduce biases in streamline densities (Smith et al., 2015), respectively, leading to more interpretable results. Nonetheless, this correction is not perfect and brain network metrics computed on SC were previously shown to be affected by the methods used to perform tractogram bias correction (Yeh et al., 2016). In particular, a bias towards over-represented long fibers might lead to a decreased coupling for localized brain systems involving short connections, which, however, does not seem to occur in our case and in previous analyses of SDI (e.g., highly coupled visual / auditory systems; (Preti and Van De Ville, 2019; Griffa et al., 2021). Nonetheless, the effect of different SC processing choices could be worth evaluating in future work.

Furthermore, tractography reconstructions can be influenced by a number of factors, such as movement, that might lead to confounds. To overcome this, we employed state-of-the-art methodologies for the preprocessing of dMRI data, and we regressed out motion from our analysis. However, average within-scanner was significantly higher in patients with 22q11DS, when compared to healthy controls. We have tried to further control for the effect of motion by regressing-out motion variable from our analysis. We have further conducted a series of post-hoc analysis to ensure the results are not driven by the difference of motion across the two groups (described in detail in supplementary material). Moreover, SDI methodology gives a nodal summary measure for each region. Therefore, this highlights regions with overall changes, without providing information on specific connection alterations. Contrary to the previous work (Preti and Van De Ville, 2019) in which the relationship between brain structure and function was investigated using the structural connectome at the group level, in the present study the structural connectome of each subject has been taken into account. This permitted characterizing the alignment of brain function and anatomy at the individual level and to correlate for each patient the FSD pattern with the severity of positive psychotic symptoms.

To the best of our knowledge this is the first study to assess the SDI alterations in a pathologic group. We have quantified the differences of functional-structural dependency across the brains of patients with 22q11DS and further evaluated how these changes are correlated with positive psychotic symptoms. Indeed, the method employed here does not provide direct information regarding the underlying neurobiological changes. However, our results revealed higher FSD in patients with 22q11DS, occurring mainly in hyperactive regions known to be segregated from higher order cortices. Conversely, lower FSD in patients with 22q11DS coincided with regions that are known to go through abnormal pruning and form suboptimal connections. Future studies on SDI alterations in pathologic populations may provide further insight into the biological correlates of SDI. Moreover, studies characterizing the age dependent trajectories of SDI may shed light on how dependency of functional activity over structural underlay changes across the development.

CRediT authorship contribution statement

Karin Bortolin: Conceptualization, Investigation, Methodology, Formal analysis, Software, Writing – original draft, Visualization. **Farnaz Delavari:** Conceptualization, Investigation, Methodology, Formal analysis, Software, Writing – original draft, Visualization. **Maria Giulia Preti:** Conceptualization, Methodology, Software, Writing – review & editing. **Corrado Sandini:** Conceptualization, Writing – review & editing. **Valentina Mancini:** Investigation, Writing – review & editing. **Emeline Mullier:** Methodology, Software, Writing – review & editing. **Dimitri Van De Ville:** Conceptualization, Resources, Methodology, Writing – review & editing, Supervision, Project administration, Funding acquisition. **Stephan Eliez:** Conceptualization, Investigation, Resources, Writing – review & editing, Supervision, Project administration, Funding acquisition.

Declaration of Competing Interest

The authors declare that they have no known competing financial interests or personal relationships that could have appeared to influence the work reported in this paper.

Acknowledgments

Swiss National Science Foundation (Grant No. 320030_179404 and 324730_144260 [to SE]) and a National Centre of Competence in Research Synapsy grant (Grant No. 51NF40-185897 [to SE]) supported the current work. MGP was supported by the CIBM Center for Biomedical Imaging, a Swiss research center of excellence founded and supported by Lausanne University Hospital (CHUV), University of Lausanne (UNIL), Ecole polytechnique fédérale de Lausanne (EPFL), University of Geneva (UNIGE) and Geneva University Hospitals (HUG).

We are grateful to all the families who participated in our study and would like to thank Eva Micol for coordinating the project, the MRI operators at the CIBM Center for Biomedical Imaging, François Lazeyras, Mery Gavillet, Caren Latreche, Velia Decoro for their precious help during data collection.

Appendix A. Supplementary data

Supplementary data to this article can be found online at https://doi.org/10.1016/j.nicl.2022.103075.

References

McClellan, J., 2018. Psychosis in Children and Adolescents. J. Am. Acad. Child Adolesc. Psychiatry 57 (5), 308–312.
Gore, F.M., Bloem, P.JN., Patton, G.C., Ferguson, J., Joseph, V., Coffey, C., Sawyer, S.M., Mathers, C.D., 2011. Global burden of disease in young people aged 10–24 years: A systematic analysis. Lancet 377 (9783), 2093–2102.
Kendler, K.S., 2013. What psychiatric genetics has taught us about the nature of psychiatric illness and what is left to learn. Mol. Psychiatry 18 (10), 1058–1066.
Biswas, A.B., Furniss, F., 2016. Cognitive phenotype and psychiatric disorder in 22q11.2 deletion syndrome: A review. Res. Dev. Disabil. 53-54, 242–257.
Murphy, K.C., Jones, L.A., Owen, M.J., 1999. High rates of schizophrenia in adults with velo-cardio-facial syndrome. Arch. Gen. Psychiatry 56 (10), 940.
Lewandowski, K.E., Shashi, V., Berry, P.M., Kwapil, T.R., 2007. Schizophrenic-like neurocognitive deficits in children and adolescents with 22q11 deletion syndrome. Am. J. Med. Genet. Part B Neuropsychiatr. Genet. 144B (1), 27–36.
Schneider, M., Schaer, M., Mutlu, A.K., Menghetti, S., Glaser, B., Debbané, M., Eliez, S., 2014. Clinical and cognitive risk factors for psychotic symptoms in 22q11.2 deletion syndrome: a transversal and longitudinal approach. Eur. Child Adolesc. Psychiatry 23 (6), 425–436.
Schneider, M., Debbané, M., Bassett, A.S., Chow, E.W.C., Fung, W.L.A., van den Bree, M. B.M., Owen, M., Murphy, K.C., Niarchou, M., Kates, W.R., Antshel, K.M., Fremont, W., McDonald-McGinn, D.M., Gur, R.E., Zackai, E.H., Vorstman, J., Duijff, S.N., Klaassen, P.W.J., Swillen, A., Gothelf, D., Green, T., Weizman, A., Van Amelsvoort, T., Evers, L., Boot, E., Shashi, V., Hooper, S.R., Bearden, C.E., Jalbrzikowski, M., Armando, M., Vicari, S., Murphy, D.G., Ousley, O., Campbell, L. E., Simon, T.J., Eliez, S., 2014. Psychiatric disorders from childhood to adulthood in 22q11.2 deletion syndrome: Results from the international consortium on brain and behavior in 22q11.2 deletion syndrome. Am. J. Psychiatry 171 (6), 627–639.
McDonald-McGinn, D.M., Sullivan, K.E., Marino, B., Philip, N., Swillen, A., Vorstman, J. A.S., Zackai, E.H., Emanuel, B.S., Vermeesch, J.R., Morrow, B.E., Scambler, P.J., Bassett, A.S., 2015. 22q11.2 deletion syndrome. Nat. Rev. Dis Prim. 1 (1) https://doi.org/10.1038/nrdp.2015.71.
Insel, T.R., 2010. Rethinking schizophrenia. Nature 468 (7321), 187–193.
Lewis, D.A., Levitt, P., 2002. Schizophrenia as a disorder of neurodevelopment. Annu. Rev. Neurosci. 25 (1), 409–432.
Johnson, M.H., 2001. Functional brain development in humans. Nat. Rev. Neurosci. 2 (7), 475–483.
Fornito, A., Zalesky, A., Pantelis, C., Bullmore, E.T., 2012. Schizophrenia, neuroimaging and connectomics. NeuroImage 62 (4), 2296–2314.
Pettersson-Yeo, W., Allen, P., Benetti, S., McGuire, P., Mechelli, A., 2011. Dysconnectivity in schizophrenia: Where are we now? Neurosci. Biobehav. Rev. 35 (5), 1110–1124.
Stephan, K.E., Friston, K.J., Frith, C.D., 2009. Dysconnection in Schizophrenia: From abnormal synaptic plasticity to failures of self-monitoring. Schizophr. Bull. 35 (3), 509–527.
McGuire, P.K., Frith, C.D., 1996. Disordered functional connectivity in schizophrenia. Psychol. Med. 26 (4), 663–667.
Lawrie, S.M., Buechel, C., Whalley, H.C., Frith, C.D., Friston, K.J., Johnstone, E.C., 2002. Reduced frontotemporal functional connectivity in schizophrenia associated with auditory hallucinations. Biol. Psychiatry 51 (12), 1008–1011.
Karbasforoushan, H., Woodward, N.D., 2013. Resting-State Networks in Schizophrenia. Curr. Top. Med. Chem. https://doi.org/10.2174/1568026611212210011.
Narr, K.L., Leaver, A.M., 2015. Connectome and schizophrenia. Current Opinion in Psychiatry 28 (3), 229–235.
Stiso, J., Bassett, D.S., 2018. Spatial Embedding Imposes Constraints on Neuronal Network Architectures. Trends in Cognitive Sciences 22 (12), 1127–1142.
Hermundstad, A.M., Bassett, D.S., Brown, K.S., Aminoff, E.M., Clewett, D., Freeman, S., Frithsen, A., Johnson, A., Tipper, C.M., Miller, M.B., Grafton, S.T., Carlson, J.M., 2013. Structural foundations of resting-state and task-based functional connectivity in the human brain. Proc. Natl. Acad. Sci. U. S. A. 110 (15), 6169–6174.
Deco, G., Ponce-Alvarez, A., Mantini, D., Romani, G.L., Hagmann, P., Corbetta, M., 2013. Resting-state functional connectivity emerges from structurally and dynamically shaped slow linear fluctuations. J. Neurosci. 33 (27), 11239–11252.
Honey, C.J., Thivierge, J.-P., Sporns, O., 2010. Can structure predict function in the human brain? NeuroImage 52 (3), 766–776.
Honey, C.J., Sporns, O., Cammoun, L., Gigandet, X., Thiran, J.P., Meuli, R., Hagmann, P., 2009. Predicting human resting-state functional connectivity from structural connectivity. Proc Natl Acad Sci U S A 106 (6), 2035–2040.
Sporns, O., Tononi, G., Kötter, R., 2005. The human connectome: A structural description of the human brain. PLoS Comput. Biol. 1 (4), e42.
Suárez, L.E., Markello, R.D., Betzel, R.F., Misic, B., 2020. Linking Structure and Function in Macroscale Brain Networks. Trends in Cognitive Sciences 24 (4), 302–315.
van den Heuvel, M.P., Sporns, O., Collin, G., Scheewe, T., Mandl, R.C.W., Cahn, W., Goñi, J., Hulshoff Pol, H.E., Kahn, R.S., 2013. Abnormal rich club organization and functional brain dynamics in schizophrenia. JAMA Psychiatry 70 (8), 783.
Skudlarski, P., Jagannathan, K., Anderson, K., Stevens, M.C., Calhoun, V.D., Skudlarska, B.A., Pearlson, G., 2010. Brain Connectivity Is Not Only Lower but Different in Schizophrenia: A Combined Anatomical and Functional Approach. Biol. Psychiatry 68 (1), 61–69.
Cocchi, L., Harding, I.H., Lord, A., Pantelis, C., Yucel, M., Zalesky, A., 2014. Disruption of structure-function coupling in the schizophrenia connectome. NeuroImage Clin 4, 779–787.
Crossley, N.A., Mechelli, A., Ginestet, C., Rubinov, M., Bullmore, E.T., McGuire, P., 2016. Altered hub functioning and compensatory activations in the connectome: A meta-Analysis of functional neuroimaging studies in schizophrenia. Schizophr. Bull. 42 (2), 434–442.
Atasoy, S., Deco, G., Kringelbach, M.L., Pearson, J., 2018. Harmonic Brain Modes: A Unifying Framework for Linking Space and Time in Brain Dynamics. Neuroscientist 24 (3), 277–293.
Huang, W., Bolton, T.A.W., Medaglia, J.D., Bassett, D.S., Ribeiro, A., Van De Ville, D., 2018. A Graph Signal Processing Perspective on Functional Brain Imaging. Proc. IEEE 106 (5), 868–885.

Preti, M.G., Van De Ville, D., 2019. Decoupling of brain function from structure reveals regional behavioral specialization in humans. Nat. Commun. 10 (1) https://doi.org/10.1038/s41467-019-12765-7.
Medaglia, J.D., Huang, W., Karuza, E.A., Kelkar, A., Thompson-Schill, S.L., Ribeiro, A., Bassett, D.S., 2018. Functional alignment with anatomical networks is associated with cognitive flexibility. Nat. Hum. Behav. 2 (2), 156–164.
Mattiaccio, L.M., Coman, I.L., Thompson, C.A., Fremont, W.P., Antshel, K.M., Kates, W. R., 2018. Frontal dysconnectivity in 22q11.2 deletion syndrome: An atlas-based functional connectivity analysis. Behav Brain Funct. 14 (1) https://doi.org/10.1186/s12993-018-0134-y.
Ottet, M.C., Schaer, M., Cammoun, L., Schneider, M., Debbané, M., Thiran, J.P., Eliez, S. (2013): Reduced Fronto-Temporal and Limbic Connectivity in the 22q11.2 Deletion Syndrome: Vulnerability Markers for Developing Schizophrenia? *PLoS One*. https://doi.org/10.1371/journal.pone.0058429.
Scariati, E., Schaer, M., Richiardi, J., Schneider, M., Debbané, M., Van De Ville, D., Eliez, S., 2014. Identifying 22q11.2 Deletion Syndrome and Psychosis Using Resting-State Connectivity Patterns. Brain Topogr. 27 (6), 808–821.
Watkins, M.W., 2006. Orthogonal higher order structure of the Wechsler Intelligence Scale for Children–. Psychol. Assess. 18, 123.
Wechsler D (1955): Wechsler adult intelligence scale–.
Reich, W., 2000. Diagnostic Interview for Children and Adolescents (DICA). J. Am. Acad. Child Adolesc. Psychiatry 39 (1), 59–66.
Kaufman, JOAN, Birmaher, BORIS, Brent, DAVID, Rao, UMA, Flynn, CYNTHIA, Moreci, PAULA, Williamson, DOUGLAS, Ryan, NEAL, 1997. Schedule for affective disorders and schizophrenia for school-age children-present and lifetime version (K-SADS-PL): Initial reliability and validity data. J. Am. Acad. Child Adolesc. Psychiatry 36 (7), 980–988.
First, M.B., Spitzer, R.L., Gibbon, M., Williams, J.B.W., 1997. User's Guide for the Structured Clinical Interview for DSM-IV Axis I Disorders SCID-I. *Clinician Version*. American Psychiatric Pub.
Ashburner, J., Friston, K.J., 2005. Unified segmentation. Neuroimage 26 (3), 839–851.
Power, J.D., Barnes, K.A., Snyder, A.Z., Schlaggar, B.L., Petersen, S.E., 2012. Spurious but systematic correlations in functional connectivity MRI networks arise from subject motion. Neuroimage 59 (3), 2142–2154.
Jenkinson, M., Beckmann, C.F., Behrens, T.E.J., Woolrich, M.W., Smith, S.M., 2012. FSL - Review. Neuroimage.
Veraart, J., Fieremans, E., Novikov, D.S., 2016. Diffusion MRI noise mapping using random matrix theory. Magn. Reson. Med. 76 (5), 1582–1593.
Veraart, J., Novikov, D.S., Christiaens, D., Ades-aron, B., Sijbers, J., Fieremans, E., 2016. Denoising of diffusion MRI using random matrix theory. Neuroimage 142, 394–406.
Cordero-Grande, L., Christiaens, D., Hutter, J., Price, A.N., Hajnal, J.V., 2019. Complex diffusion-weighted image estimation via matrix recovery under general noise models. Neuroimage 200, 391–404.
Andersson, J.L.R., Sotiropoulos, S.N., 2016. An integrated approach to correction for off-resonance effects and subject movement in diffusion MR imaging. Neuroimage 125, 1063–1078.
Avants, B., Epstein, C., Grossman, M., Gee, J., 2008. Symmetric diffeomorphic image registration with cross-correlation: Evaluating automated labeling of elderly and neurodegenerative brain. Med. Image Anal. 12 (1), 26–41.
Andersson, J.L.R., Jenkinson, M., Smith, S., 2007. Non-linear registration aka spatial normalisation. FMRIB Technical Report TRO7JA2.
Tournier, J.-D., Calamante, F., Connelly, A., 2007. Robust determination of the fibre orientation distribution in diffusion MRI: Non-negativity constrained super-resolved spherical deconvolution. Neuroimage 35 (4), 1459–1472.
Smith, R.E., Tournier, J.-D., Calamante, F., Connelly, A., 2012. Anatomically-constrained tractography: Improved diffusion MRI streamlines tractography through effective use of anatomical information. Neuroimage 62 (3), 1924–1938.
Smith, R.E., Tournier, J.-D., Calamante, F., Connelly, A., 2015. SIFT2: Enabling dense quantitative assessment of brain white matter connectivity using streamlines tractography. Neuroimage 119, 338–351.
Benjamini, Y., Hochberg, Y., 1995. Controlling the False Discovery Rate: A Practical and Powerful Approach to Multiple Testing. J R Stat Soc Ser B 57 (1), 289–300.
McIntosh AR, Lobaugh NJ (2004): Partial least squares analysis of neuroimaging data: Applications and advances. *NeuroImage*. https://doi.org/10.1016/j.neuroimage.2004.07.020.
Krishnan, A., Williams, L.J., McIntosh, A.R., Abdi, H., 2011. Partial Least Squares (PLS) methods for neuroimaging: A tutorial and review. Neuroimage 56 (2), 455–475.
Margulies, D.S., Ghosh, S.S., Goulas, A., Falkiewicz, M., Huntenburg, J.M., Langs, G., Bezgin, G., Eickhoff, S.B., Castellanos, F.X., Petrides, M., Jefferies, E., Smallwood, J., 2016. Situating the default-mode network along a principal gradient of macroscale cortical organization. Proc Natl Acad Sci U S A 113 (44), 12574–12579.
Vázquez-Rodríguez, B., Suárez, L.E., Markello, R.D., Shafiei, G., Paquola, C., Hagmann, P., van den Heuvel, M.P., Bernhardt, B.C., Spreng, R.N., Misic, B., 2019. Gradients of structure–function tethering across neocortex. Proc Natl Acad Sci U S A 116 (42), 21219–21227.
Baum, G.L., Cui, Z., Roalf, D.R., Ciric, R., Betzel, R.F., Larsen, B., Cieslak, M., Cook, P.A., Xia, C.H., Moore, T.M., Ruparel, K., Oathes, D.J., Alexander-Bloch, A.F., Shinohara, R.T., Raznahan, A., Gur, R.E., Gur, R.C., Bassett, D.S., Satterthwaite, T.D., 2020. Development of structure–function coupling in human brain networks during youth. Proc Natl Acad Sci U S A 117 (1), 771–778.
Paquola, C., Vos De Wael, R., Wagstyl, K., Bethlehem, R.A.I., Hong, S.-J., Seidlitz, J., Bullmore, E.T., Evans, A.C., Misic, B., Margulies, D.S., Smallwood, J., Bernhardt, B. C., Kennedy, H., 2019. Microstructural and functional gradients are increasingly dissociated in transmodal cortices. PLoS Biol. 17 (5), e3000284.
Buckner, R.L., Krienen, F.M., 2013. The evolution of distributed association networks in the human brain. Trends in Cognitive Sciences 17 (12), 648–665.
Bettinardi, R.G., Deco, G., Karlaftis, V.M., Van Hartevelt, T.J., Fernandes, H.M., Kourtzi, Z., Kringelbach, M.L., Zamora-López, G., 2017. How structure sculpts function: Unveiling the contribution of anatomical connectivity to the brain's spontaneous correlation structure. Chaos. doi 27 (4), 047409.
Damoiseaux, J.S., Greicius, M.D., 2009. Greater than the sum of its parts: A review of studies combining structural connectivity and resting-state functional connectivity. Brain Struct. Funct. 213 (6), 525–533.
Mesulam, M., 1998. From sensation to cognition. Brain 121 (6), 1013–1052.
Utter, A.A., Basso, M.A., 2008. The basal ganglia: An overview of circuits and function. Neurosci. Biobehav. Rev. 32 (3), 333–342.
Berridge, K., Kringelbach, M., 2015. Pleasure Systems in the Brain. Neuron 86 (3), 646–664.
Janak, P.H., Tye, K.M., 2015. From circuits to behaviour in the amygdala. Nature 517 (7534), 284–292.
Miller, E.K., Cohen, J.D., 2001. An integrative theory of prefrontal cortex function. Annu. Rev. Neurosci. 24 (1), 167–202.
Kolb, B., Gibb, R., 2011. Brain Plasticity and Behaviour in the Developing Brain. Journal of the Canadian Academy of Child and Adolescent Psychiatry.
Hooper, C.J., Luciana, M., Conklin, H.M., Yarger, R.S., 2004. Adolescents' performance on the iowa gambling task: Implications for the development of decision making and ventromedial prefrontal cortex. Dev. Psychol. 40 (6), 1148–1158.
Mills, K.L., Goddings, A.-L., Clasen, L.S., Giedd, J.N., Blakemore, S.-J., 2014. The developmental mismatch in structural brain maturation during adolescence. Dev. Neurosci. 36 (3-4), 147–160.
Schlegel AA, Rudelson JJ, Tse PU (2012): White matter structure changes as adults learn a second language. *J Cogn Neurosci*. https://doi.org/10.1162/jocn_a_00240.
Shashi, V., Veerapandiyan, A., Keshavan, M.S., Zapadka, M., Schoch, K., Kwapil, T.R., Hooper, S.R., Stanley, J.A., 2012. Altered Development of the Dorsolateral Prefrontal Cortex in Chromosome 22q11.2 Deletion Syndrome: An In Vivo Proton Spectroscopy Study. Biol. Psychiatry 72 (8), 684–691.
Schaer, M., Debbané, M., Bach Cuadra, M., Ottet, M.-C., Glaser, B., Thiran, J.-P., Eliez, S., 2009. Deviant trajectories of cortical maturation in 22q11.2 deletion syndrome (22q11DS): A cross-sectional and longitudinal study. Schizophr. Res. 115 (2-3), 182–190.
Radoeva, P.D., Coman, I.L., Antshel, K.M., Fremont, W., McCarthy, C.S., Kotkar, A., Wang, D., Shprintzen, R.J., Kates, W.R., 2012. Atlas-based white matter analysis in individuals with velo-cardio-facial syndrome (22q11.2 deletion syndrome) and unaffected siblings. Behav Brain Funct. 8 (1) https://doi.org/10.1186/1744-9081-8-38.
Schreiner, M.J., Karlsgodt, K.H., Uddin, L.Q., Chow, C., Congdon, E., Jalbrzikowski, M., Bearden, C.E., 2014. Default mode network connectivity and reciprocal social behavior in 22q11.2 deletion syndrome. Soc Cogn Affect Neurosci 9 (9), 1261–1267.
Lodge, D.J., Grace, A.A., 2007. Aberrant hippocampal activity underlies the dopamine dysregulation in an animal model of schizophrenia. J. Neurosci. 27 (42), 11424–11430.
Delavari, F., Sandini, C., Zöller, D., Mancini, V., Bortolin, K., Schneider, M., Van De Ville, D., Eliez, S., 2021. Dysmaturation observed as altered hippocampal functional connectivity at rest is associated with the emergence of positive psychotic symptoms in patients with 22q11 deletion syndrome. Biol. Psychiatry 90 (1), 58–68.
Rihs, T.A., Tomescu, M.I., Britz, J., Rochas, V., Custo, A., Schneider, M., Debbané, M., Eliez, S., Michel, C.M., 2013. Altered auditory processing in frontal and left temporal cortex in 22q11.2 deletion syndrome: A group at high genetic risk for schizophrenia. Psychiatry Research: Neuroimaging 212 (2), 141–149.
Scariati, E., Padula, M.C., Schaer, M., Eliez, S., 2016. Long-range dysconnectivity in frontal and midline structures is associated to psychosis in 22q11.2 deletion syndrome. J. Neural Transm. 123 (8), 823–839.
Sandini, C., Scariati, E., Padula, M.C., Schneider, M., Schaer, M., Van De Ville, D., Eliez, S., 2018. Cortical Dysconnectivity Measured by Structural Covariance Is Associated With the Presence of Psychotic Symptoms in 22q11.2 Deletion Syndrome. Biological Psychiatry: Cognitive Neuroscience and Neuroimaging 3 (5), 433–442.
Tomescu, M.I., Rihs, T.A., Becker, R., Britz, J., Custo, A., Grouiller, F., Schneider, M., Debbané, M., Eliez, S., Michel, C.M., 2014. Deviant dynamics of EEG resting state pattern in 22q11.2 deletion syndrome adolescents: A vulnerability marker of schizophrenia? Schizophr. Res. 157 (1-3), 175–181.
Padula MC, Scariati E, Schaer M, Eliez S (2018): A mini review on the contribution of the anterior cingulate cortex in the risk of psychosis in 22q11.2 deletion syndrome. *Frontiers in Psychiatry*. https://doi.org/10.3389/fpsyt.2018.00372.
Allen, P., Larøi, F., McGuire, P.K., Aleman, A., 2008. The hallucinating brain: A review of structural and functional neuroimaging studies of hallucinations. Neurosci. Biobehav. Rev. 32 (1), 175–191.
Menon, V., 2011. Large-scale brain networks and psychopathology: A unifying triple network model. Trends in Cognitive Sciences 15 (10), 483–506.
Kapur, S., 2003. Psychosis as a state of aberrant salience: A framework linking biology, phenomenology, and pharmacology in schizophrenia. Am. J. Psychiatry 160 (1), 13–23.
Witter, M.P., Wouterlood, F.G., Naber, P.A., Van haeften, THEO, 2000. Anatomical organization of the parahippocampal-hippocampal network. Ann. N. Y. Acad. Sci. 911 (1), 1–24.
Rolls, E.T., 2019. The cingulate cortex and limbic systems for emotion, action, and memory. Brain Struct. Funct. 224 (9), 3001–3018.
Arnold OH (1999): Schizophrenia - A disturbance of signal interaction between the entorhinal cortex and the dentate gyrus? The contribution of experimental dibenamine psychosis to the pathogenesis of schizophrenia: A hypothesis. *Neuropsychobiology*. https://doi.org/10.1159/000026593.

Falkai, P., Schneider-Axmann, T., Honer, W.G., 2000. Entorhinal cortex pre-alpha cell clusters in schizophrenia: Quantitative evidence of a developmental abnormality. Biol. Psychiatry 47 (11), 937–943.

Prasad, K.M.R., Patel, A.R., Muddasani, S., Sweeney, J., Keshavan, M.S., 2004. The entorhinal cortex in first-episode psychotic disorders: A structural magnetic resonance imaging study. Am. J. Psychiatry 161 (9), 1612–1619.

Zöller, D., Schaer, M., Scariati, E., Padula, M.C., Eliez, S., Van De Ville, D., 2017. Disentangling resting-state BOLD variability and PCC functional connectivity in 22q11.2 deletion syndrome. Neuroimage. 149, 85–97.

Boley, A.M., Perez, S.M., Lodge, D.J., 2014. A fundamental role for hippocampal parvalbumin in the dopamine hyperfunction associated with schizophrenia. Schizophr. Res. 157 (1-3), 238–243.

Friston, K.J., Liddle, P.F., Frith, C.D., Hirsch, S.R., Frackowiak, R.S.J., 1992. The left medial temporal region and schizophrenia: A pet study. Brain 115 (2), 367–382.

Lisman, J.E., Otmakhova, N.A., 2001. Storage, recall, and novelty detection of sequences by the hippocampus: Elaborating on the SOCRATIC model to account for normal and aberrant effects of dopamine. Hippocampus 11 (5), 551–568.

Larsen, K.M., Dzafic, I., Siebner, H.R., Garrido, M.I., 2019. Alteration of functional brain architecture in 22q11.2 deletion syndrome – Insights into susceptibility for psychosis. NeuroImage. 190, 154–171.

Bostelmann, M., Schneider, M., Padula, M.C., Maeder, J., Schaer, M., Scariati, E., Debbané, M., Glaser, B., Menghetti, S., Eliez, S., 2016. Visual memory profile in 22q11.2 microdeletion syndrome: Are there differences in performance and neurobiological substrates between tasks linked to ventral and dorsal visual brain structures? A cross-sectional and longitudinal study. J Neurodev Disord. 8 (1) https://doi.org/10.1186/s11689-016-9174-5.

Attout, L., Noël, M.-P., Vossius, L., Rousselle, L., 2017. Evidence of the impact of visuo-spatial processing on magnitude representation in 22q11.2 microdeletion syndrome. Neuropsychologia. 99, 296–305.

Mancini, V., Zöller, D., Schneider, M., Schaer, M., Eliez, S., 2020. Abnormal Development and Dysconnectivity of Distinct Thalamic Nuclei in Patients With 22q11.2 Deletion Syndrome Experiencing Auditory Hallucinations. Biological Psychiatry: Cognitive Neuroscience and Neuroimaging 5 (9), 875–890.

Ferri, J., Ford, J.M., Roach, B.J., Turner, J.A., van Erp, T.G., Voyvodic, J., Preda, A., Belger, A., Bustillo, J., O'Leary, D., Mueller, B.A., Lim, K.O., McEwen, S.C., Calhoun, V.D., Diaz, M., Glover, G., Greve, D., Wible, C.G., Vaidya, J.G., Potkin, S.G., Mathalon, D.H., 2018. Resting-state thalamic dysconnectivity in schizophrenia and relationships with symptoms. Psychol. Med. 48 (15), 2492–2499.

Li, B., Cui, L.-B., Xi, Y.-B., Friston, K.J., Guo, F., Wang, H.-N., Zhang, L.-C., Bai, Y.-H., Tan, Q.-R., Yin, H., Lu, H., 2017. Abnormal Effective Connectivity in the Brain is Involved in Auditory Verbal Hallucinations in Schizophrenia. Neurosci Bull 33 (3), 281–291.

Calamuneri, A., Arrigo, A., Mormina, E., Milardi, D., Cacciola, A., Chillemi, G., Marino, S., Gaeta, M., Quartarone, A., 2018. White matter tissue quantification at Low b-values within constrained spherical deconvolution framework. Front. Neurol. 9 https://doi.org/10.3389/fneur.2018.00716.

Tournier, J.-D., Calamante, F., Gadian, D.G., Connelly, A., 2004. Direct estimation of the fiber orientation density function from diffusion-weighted MRI data using spherical deconvolution. Neuroimage 23 (3), 1176–1185.

Smith, R.E., Tournier, J.-D., Calamante, F., Connelly, A., 2015. The effects of SIFT on the reproducibility and biological accuracy of the structural connectome. Neuroimage 104, 253–265.

Yeh, C.-H., Smith, R.E., Liang, X., Calamante, F., Connelly, A., 2016. Correction for diffusion MRI fibre tracking biases: The consequences for structural connectomic metrics. Neuroimage 142, 150–162.

Griffa A, Amico E, Liégeois R, De Ville D Van, Preti MG (2021): Structure-function interplay as signature for brain decoding and fingerprinting. *bioRxiv*.